1 **The spatial distribution and temporal drivers of changing global fire regimes: a**
2 **coupled socio-ecological modelling approach**

3 **Oliver Perkins[1,2], Matthew Kasoar[1,3], Apostolos Voulgarakis[1,3,4], Tamsin Edwards[2], and**
4 **James Millington[1,2]**

5 [1]The Leverhulme Centre for Wildfires, Environment, and Society, Imperial College London,
6 SB7 2BX, UK, [2]Department of Geography, King's College London, WC2B 4BG, UK,
7 [3]Department of Physics, Imperial College London, [4]School of Chemical and Environmental
8 Engineering, Technical University of Crete, Kounoupidiana, 73100, Greece

9 Corresponding author: Oliver Perkins (oliver.perkins@kcl.ac.uk)

10

11 **Key Points:**

12 • Representing managed fire in global-scale fire models has represented a substantial
13   research challenge in fire science

14 • We address this through the offline coupling of a global agent-based model of human fire
15   use with a dynamic global vegetation model

16 • The coupling improves performance of modelled burned area and allows exploration of
17   drivers of change in global fire regimes

18 **Abstract**

19 In the Anthropocene, humans are the largest drivers of change in vegetation fire regimes.
20 Humans influence fire regimes both directly, by starting, managing and extinguishing fires, and
21 also indirectly by altering fuel composition and connectivity. However, whilst vegetation fire is a
22 coupled socio-ecological process, representation of human influences on fire regimes in global-
23 scale modelling remains limited. This places a fundamental constraint on our ability to
24 understand how human and natural processes combine to create observed patterns of vegetation
25 fire, and how such processes may interact under future scenarios of socioeconomic and
26 environmental change. Here, we respond to this challenge by presenting a novel integration of
27 two global and process-based models. The first is the Wildfire Human Agency Model
28 (WHAM!), which draws on agent-based approaches to represent anthropogenic fire use and
29 management. The second is JULES-INFERNO, a fire-enabled dynamic global vegetation model,
30 which takes a physically-grounded approach to the representation of vegetation-fire dynamics.
31 The WHAM-INFERNO combined model suggests that as much as half of all global burned area
32 is generated by managed anthropogenic fires – typically small fires that are lit and then spread
33 according to land user objectives. Furthermore, we demonstrate that including representation of
34 managed anthropogenic fires in a coupled socio-ecological simulation can improve
35 understanding of the drivers of unmanaged wildfires. Overall, findings presented here have
36 substantial implications for understanding of present-day and future fire regimes, indicating that
37 socio-economic change may be as important as climate change in determining the future
38 trajectory of fire on Earth.
39

40 **Plain Language Summary**
41 For millennia, humans have used fire as a tool to manage land and they continue to do so across
42 the world today. However, global-scale models which are used to understand how vegetation fire
43 may respond to climate change have not yet robustly accounted for this. So, we built a new
44 model that represents how humans use and manage fire globally and coupled it with a global fire
45 model. We find that improved representation of human impacts on fire significantly improves the
46 model and sheds new light on what is driving change in vegetation fire globally. In particular,
47 our results suggest current global fire models may have underestimated the sensitivity of fire to
48 climate change.
49

1 Introduction

Vegetation fire is a coupled socio-ecological process, in which humans are the largest driver of change in its global distribution (Andela et al., 2017; Kelley et al., 2019). Perhaps the central example of this is that, whilst the planet has warmed under recent anthropogenic climate change, the area burned globally each year has decreased, particularly in savannas and grasslands (Chen et al., 2023). Drivers of this phenomenon are complex and uncertain (Zubkova et al., 2023), ranging from cropland conversion (Andela et al., 2017) to changes in anthropogenic fire use (Smith et al., 2022), from increased grazing intensity (Archibald & Hempson, 2016) to the CO_2 fertilisation effect (Ripley et al., 2022; Stevens et al., 2016). A lack of clarity around the drivers of declining global burned area has made attribution of changes in global fire regimes a significant challenge (Jones et al., 2022). This, in turn, limits understanding of how fire may evolve in the future, including its potential role as a positive feedback to climate change (Lasslop et al., 2019).

At the heart of this uncertainty are the huge diversity of ways in which humans use and manage fire. Human fire use ranges from burning of agricultural residues in intensive land use systems (Kumar et al., 2023) to cultural uses such as religious ceremonies (Smith et al., 2022). Human fire management is similarly diverse, ranging from pro-active indigenous 'patch-burning' methods (Laris, 2002) to industrial fire suppression. As such, fire can broadly be categorised into managed or 'landscape' fires - which are typically small, controlled, and can be beneficial to humans - and unmanaged wildfires, which are larger and burn more intensely (UNEP 2022). Furthermore, human fire use is itself undergoing substantial change, with shifts away from more subsistence-oriented fire uses (Smith et al., 2022) and possibly an overall decline in fire use driven by agricultural intensification (Perkins et al., 2023). Consequently, Shuman et al., (2022) argue that incorporating managed fire into models at all spatial scales is an important step towards equipping fire science for the Anthropocene.

In addition to direct anthropogenic influences on fire, humans also have many indirect influences on fire regimes. For example, multiple authors have argued that anthropogenic fragmentation of vegetated landscapes is a key process shaping the evolution of global fire (Archibald et al., 2012; Driscoll et al., 2021; Harrison et al., 2021). Fragmentation can have opposite effects across ecosystems – with logging and degradation increasing fire in otherwise fire-independent forests, and reduced fuel connectivity decreasing burned area in grassland and savannah ecosystems (Rosan et al., 2022). As such, understanding the drivers of change within global fire regimes requires consideration not only of biophysical factors, but also of both direct and indirect human impacts.

Global-scale fire models have struggled to reproduce the observed decline in global burned area (Hantson et al., 2020). Indeed, in the first intercomparison project of the global fire model community (FireMIP; Rabin et al., 2017), models largely disagreed about both centennial trends, and more recent decadal trends, in global burned area (Teckentrup et al., 2019). Underlying this lack of consensus have been substantial limitations in the representation of human impacts on the fire modules of dynamic global vegetation models (DGVMs; Ford et al., 2021). Typically, these have been restricted to global functions relating population density to numbers of fires in satellite observations (Rabin et al., 2017). This ignores the diversity of human fire use and management, and hence limits the capability of DGVMs to advance understanding of socio-ecological dynamics of present-day fire regimes and how human and biophysical factors may interact in the future (Shuman et al., 2022).

95   The Wildfire Human Agency Model (WHAM!; Perkins et al., 2023) is the first formal
96 model to represent present-day anthropogenic fire use and management at global scale. Drawing
97 on agent-based approaches, WHAM! is a geospatial behavioural model that captures the
98 underlying land system drivers of anthropogenic fire use and management to simulate human fire
99 use decision-making from the bottom-up (Perkins et al., 2022). As WHAM! only represents
100 human influences on global fire regimes, it was designed to be integrated with fire-enabled
101 DGVMs, such as the JULES-INFERNO model (Mangeon et al., 2016), which capture the
102 biophysical drivers of fire. Here we present the first coupling between WHAM! and JULES-
103 INFERNO, such that biophysical, direct and indirect human drivers of fire regimes are all
104 explicitly represented in an integrated simulation for the first time.

105   WHAM! takes its empirical basis from the Database of Anthropogenic Fire Impacts
106 (DAFI; Perkins & Millington, 2021). DAFI is the product of a literature meta-analysis of 1809
107 case studies from 504 academic papers, government and NGO reports (Millington et al., 2022).
108 This dataset addresses a previous barrier to improved representation of anthropogenic fire in
109 DGVMs: the lack of a systematic data set on which to base new parameterisations (Forkel et al.,
110 2019). Alongside development of DAFI, the 5th version of the Global Fire Emissions Database
111 (GFED5; Chen et al., 2023) accounts for smaller fires than previous versions and therefore
112 enables more robust evaluation of global-scale modelling of human fire interactions. Previous
113 iterations of GFED have been based on a combination of MODIS for burned area and VIRS for
114 active fire detection (Giglio et al., 2013). As such, they have not been able to systematically
115 detect anthropogenic fires: DAFI suggests that >50% of anthropogenic fires are smaller than the
116 21ha threshold above which MODIS can detect (Millington et al., 2022). GFED5 incorporates
117 higher resolution remote sensing (principally from Landsat and Sentinel-2), and hence is much
118 more effective at capturing small fires: global burned area in GFED5 is a 61% increase over
119 GFED4s (Chen et al., 2023). Therefore, with DAFI providing an empirical-basis for bottom-up
120 modelling of human-fire interactions, and GFED5 better able to detect them from space, a
121 comprehensive and empirically-grounded assessment of the role of managed anthropogenic fire
122 in global fire regimes is now possible.

123   This paper presents the integration of WHAM! with JULES-INFERNO and its
124 application to understand the spatiotemporal drivers of global fire regimes. Section 2 (Methods)
125 focuses on describing the integration of outputs from the two models. Model calibration is
126 described briefly in the main text with further details provided in Supplementary Information A.
127 In Section 3 (Results), we present a brief evaluation of the outputs of the coupled model to
128 establish its credibility, before focusing on understanding how human and biophysical factors
129 combine to produce observed distributions of fire globally. Discussion (section 4) focuses on
130 insights relevant to the question of declining global burned area, and in particular to
131 understanding the relative contribution of direct human influences (starting and suppressing
132 fires), indirect human influences (i.e. landscape fragmentation) and biophysical factors (i.e.
133 climate and vegetation flammability).
134

2 Methods

135

136   Our methods are presented in five sections, which respectively describe the inputs,
137 structure, calibration, evaluation, and analysis of the WHAM-JULES-INFERNO combined
138 model (hereafter WHAM-INFERNO). A schematic overview of the processes represented in
139 WHAM-INFERNO is presented in Figure 1. Calculations of the fire regime at each timestep
140 combine three elements: 1) WHAM! outputs for managed and unmanaged anthropogenic fires
141 and fire suppression; 2) JULES-INFERNO outputs for lightning ignitions, flammability and
142 plant functional types; and 3) a representation of vegetation fragmentation derived from
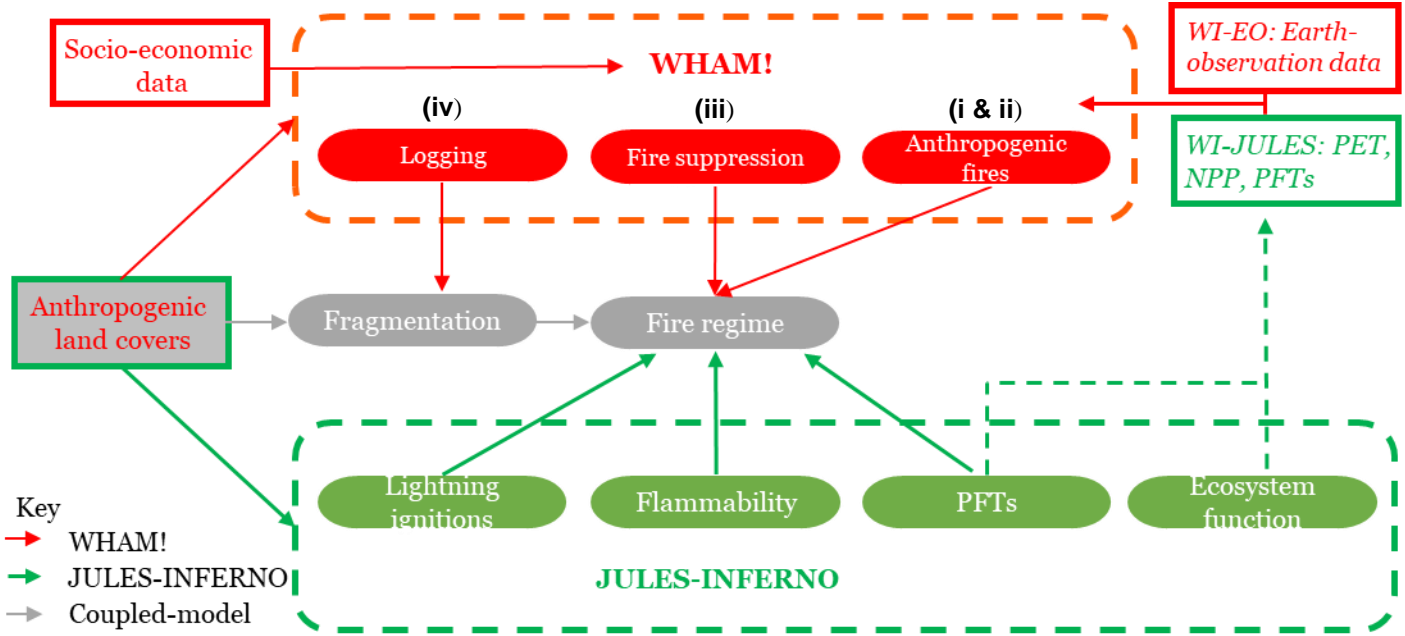143 secondary data and WHAM! outputs for logging. These are each detailed further in Section 2.1.

144   Importantly, two versions of WHAM-INFERNO are presented and assessed: WHAM-
145 INFERNO-JULES (hereafter WI-JULES) and WHAM-INFERNO-Earth Observation (hereafter
146 WI-EO). The difference between these two versions is that in WI-JULES, WHAM! is
147 parameterised using biophysical inputs directly from JULES, whilst in WI-EO, WHAM! takes
148 these inputs from remote sensing. Specifically, inputs for potential evapotranspiration, net
149 primary production and the bare soil fraction are replaced with Earth observation data. The
150 differences between these two versions of WHAM! are described in detail in Perkins et al. (2023;
151 Supplementary Information A).

152   The primary purpose of the comparison of WI-JULES and WI-EO is to allow
153 interrogation of the robustness of inferences made about the drivers of global fire regimes. For
154 example, if trends are identified in WI-JULES but not in WI-EO, then they may be attributable to
155 underlying model error in JULES' representation of ecosystem dynamics. Similarly, assessing
156 the difference in performance (as measured against GFED5) allows exploration of how far
157 underlying error in the hydrological and vegetation outputs of DGVMs may constrain the
158 capacity of their fire modules to reproduce remotely sensed observations (Hantson et al., 2020).

159   Code to run and analyse WHAM-INFERNO is written in R version 4.2.2 (R Core Team
160 2022), using the 'raster' library version 3.6-20 (Hijmans et al., 2023). Code and data to run and
161 analyse outputs of both versions of WHAM-INFERNO are made available on Zenodo (Perkins
162 et al., 2023b).

163   2.1 Inputs to the coupled model

164   WHAM-INFERNO takes inputs from WHAM!, JULES-INFERNO and from secondary
165 data sources. Each of these inputs are described in turn below (Sections 2.1.1-2.1.3), and an
166 overview is given in Table 1. WHAM! outputs are annual, whilst as per results in the sixth
167 coupled model intercomparison project (CMIP6), JULES-INFERNO outputs are aggregated
168 monthly means. Therefore, WHAM-INFERNO runs at a monthly timestep, with WHAM!
169 outputs for a given year assumed to be uniformly distributed across calendar months.

Figure 1: Processes represented in the WHAM-INFERNO combined model. Solid arrows denote dynamic model calculations, whilst dashed lines denote static exchange of information. Socio-economic data and biophysical inputs to WHAM! (Potential Evapotranspiration (PET), Net Primary Production (NPP) and Plant Functional Types (PFTs)) are passed offline. In WHAM-INFERNO-JULES (WI-JULES) these data are taken from JULES outputs, whilst in WHAM-INFERNO-Earth Observation (WI-EO) PET and NPP inputs are taken from remote sensing. Roman numerals (i-iv) correspond to numbers given in section 2.1.1 of the text.

2.1.1 WHAM! inputs to the coupled model

WHAM! inputs to the coupled model comprise i) managed burned area as a fraction of each cell, ii) numbers of unmanaged fires (count km^{-2} yr^{-1}), iii) fire suppression intensity (0-1), and iv) the presence of selective logging as a fraction of the tree cover in each cell (see corresponding numerals in Figure 1). WHAM! inputs used were those presented in Perkins et al., (2023).

2.1.2 JULES-INFERNO inputs to the coupled model

INFERNO (Mangeon et al., 2016) is the fire module of the JULES dynamic global vegetation model. INFERNO calculates burned area from fires with two key components. The first is mean global burned area per fire per Plant Functional Type (PFT), a set of PFT-specific model free parameters. Model parameters for burned area per PFT were as in Burton et al. (2019). The second component of INFERNO burned area calculations is fuel flammability, which INFERNO calculates as a function of leaf carbon and soil carbon pools, temperature, relative humidity, precipitation, and soil moisture (Mangeon et al., 2016). Flammability is therefore important in capturing the impact of both climate and spatial heterogeneity in vegetation on fire regimes. Flammability is calculated per PFT in each model pixel at each timestep. JULES outputs are from the model set-up used in CMIP6 (Wiltshire et al., 2020).

194   2.1.3 Ancillary inputs to the coupled model from secondary data

195   In addition to the calculations from the two models, three sets of secondary data were
196   used as inputs: lightning ground strikes, anthropogenic land covers – cropland, pasture,
197   rangeland and urban – and road density. Firstly, as in JULES-INFERNO standalone (Mathison et
198   al., 2023), counts of lightning strikes were sourced from the Lightning Imaging Sensor—Optical
199   Transient Detector (LIS/OTD, Christian et al., 2003). Secondly, as in CMIP6, anthropogenic
200   land cover was taken from the LUH2 dataset (Hurtt et al., 2020). Finally, Haas et al. (2022)
201   demonstrated that road density was effective in capturing vegetation fragmentation effects on fire
202   regimes at global scale; road density data were therefore taken from the GRIP global road
203   database (Meijer et al., 2018).

204

205   **Table 1**: Overview of inputs to the WHAM!-INFERNO combined model. PFT is plant
206   functional type. Data inputs for lightning strikes, road density and anthropogenic land covers
207   were rescaled to the resolution of WHAM!-INFERNO (1.875º x 1.25º). Differing temporal
208   resolutions of inputs were reconciled as noted in Section 2.1.
209

Coupled model input	Source	Units	Temporal resolution
Managed burned area	WHAM!	Cell fraction (0-1)	Annual
Unmanaged anthropogenic fires	WHAM!	Fires km^{-2}	Annual
Fire suppression	WHAM!	Cell fraction (0-1)	Annual
Selective logging	WHAM!	Cell fraction (0-1)	Annual
Distribution of PFTs	JULES-INFERNO	Cell fraction (0-1)	Monthly
Flammability per PFT	JULES-INFERNO	Dimensionless (0-1)	Monthly
Burned area per fire per PFT	JULES-INFERNO	km^2	Fixed (n/a)
Lightning – ground strikes	Christian et al., (2003)	strikes km^{-2}	Fixed (single daily mean)
Road density	Meijer et al., (2018)	m^2 km^{-2}	Annual
Anthropogenic land cover	Hurtt et al., (2020)	Cell fraction (0-1)	Annual

210
211

212   2.2 WHAM-INFERNO Structure

213   The coupled WHAM-INFERNO model is a 'prescribed' model coupling (sensu Robinson
214 et al., 2018) such that whilst simulations of global burned area depend on calculations involving
215 outputs of both models, dynamic information transfer is only one way - from WHAM! to
216 INFERNO (see Section 2.2.1). Specifically, for each simulated year, annual burned area from
217 managed fire is taken directly from WHAM!, with $\frac{1}{12}$ assigned to each calendar month. But to
218 calculate unmanaged fire burned area, the original JULES-INFERNO calculations are modified
219 by the number of anthropogenic fires (km^{-2} yr^{-1}) provided by WHAM!. Therefore, description of
220 model coupling here first describes calculation of burned area from unmanaged fires (Section
221 2.2.1). Then, as burned area from unmanaged fires is also impacted by anthropogenic landscape
222 fragmentation, the representation of such processes is then described in Section 2.2.2. Finally,
223 the calculation of overall burned area combining both managed and unmanaged fire is described
224 in Section 2.2.3.

225   2.2.1 Unmanaged fire

226   The calculation of burned area from unmanaged fires is presented in two parts: firstly the
227 calculation of numbers of unmanaged fires, and secondly the calculation of their respective
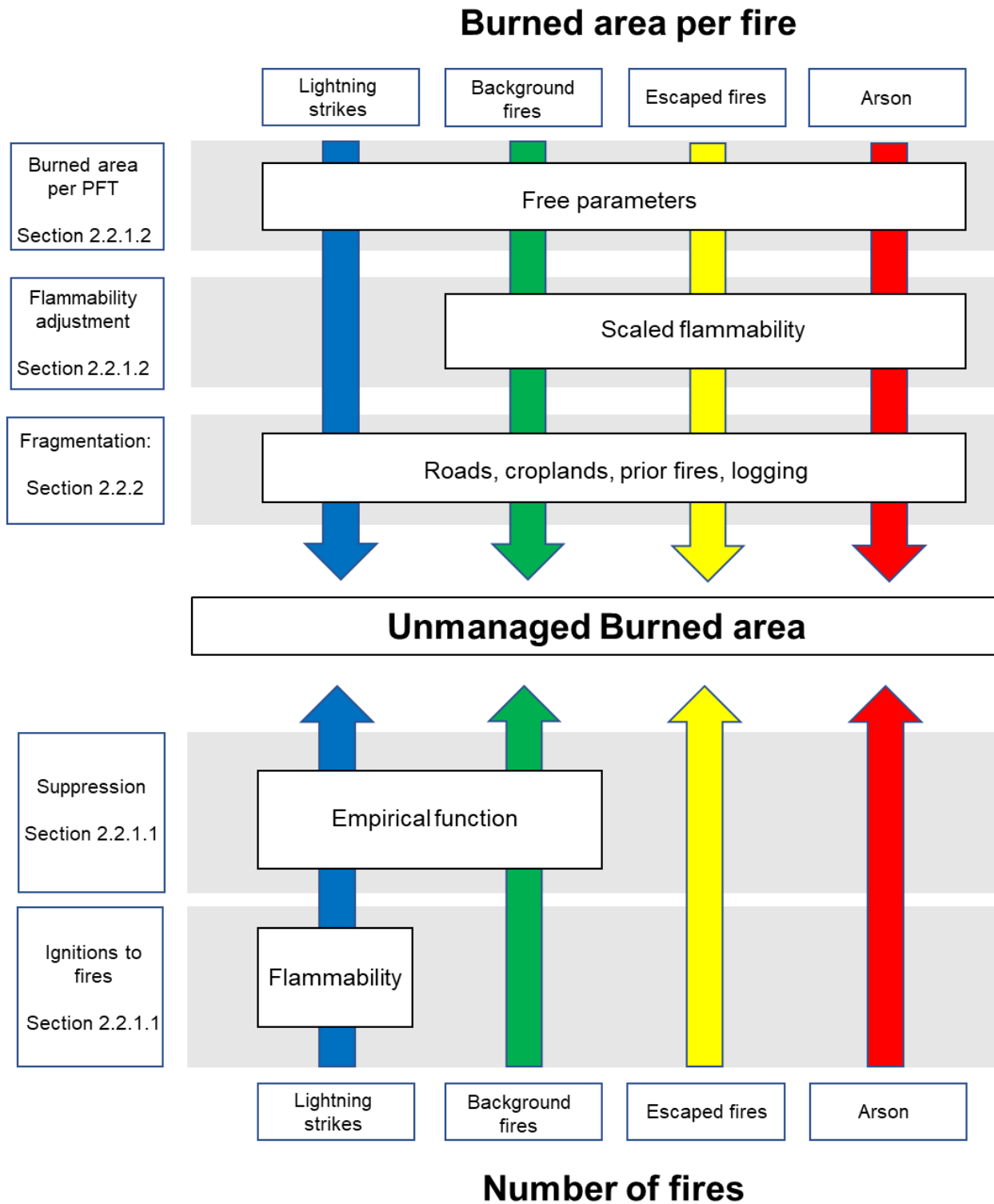228 burned area. An overview of this process is given in Figure 2.

229   2.2.1.1 Number of fires

230   In the original Mangeon et al. (2016) conception of INFERNO, the numbers of ignitions
231 from lightning strikes are calculated as follows:

232
233
$$I_L = 7.7 \times Lightning \times (1 - Suppression) \quad (1)$$

234 where I_L is the number of ignitions from lightning strikes in a given model timestep, $Lightning$
235 is the number of lightning strikes and $Suppression$ is a population density-dependent
236 suppression function. The structure of this calculation is retained with two changes: firstly, the
237 suppression function is replaced with an empirically-defined representation of suppression
238 intensity (Section 2.2.2); and secondly the empirically-defined linear scaling parameter (=7.7)
239 from Mangeon et al. (2016) is replaced with a free parameter (λ) to allow re-calibration. A
240 complete set of model free parameters is given in Supplementary Information Table S1.

Burned area per fire

Figure 2: Calculation of burned area from unmanaged fires in the WHAM-INFERNO combined model.

244   In the WHAM-INFERNO combined model, calculation of lightning fires is integrated
245   with unmanaged anthropogenic fire numbers from WHAM! as follows:

246

247    $$Fires_{UM} = Arson + Escaped + (1 - Suppression) * (Background + \ Lightning) \ (2)$$

248   where $Fires_{UM}$ is the annual number of unmanaged fires per grid box per year, $Arson$ and
249   *Escaped* fire numbers are the number of fires km^{-2} yr^{-1} taken from WHAM! outputs, and
250    $Lightning$ is the number of lightning fires calculated from mean daily ground strikes as in
251   equation (1). Finally, $Background$, is a small globally constant rate used to capture fires that
252   are not arson, lightning or escaped managed fires. The constant rate maintains an aspect of
253   INFERNO, in which a uniform 'ignition' rate is an option.

254   Fire suppression in the coupled model (Section 2.2.2) is applied to background and
255   lightning fires, but not to arson and escaped fires. This is for ontological reasons, as follows.
256   INFERNO assumes that suppressed *ignitions* have no burned area. However, in DAFI, the
257   database used to develop WHAM!'s calculation of arson and escaped *fires*, numbers of *fires* are
258   recorded, therefore by definition these have burned area > 0. As such, it is illogical to apply
259   modelled suppression to them. By contrast, as the background rate was calculated using a
260   constant, clearly this did not account for the impact of suppression. Similarly, lightning remains
261   calculated based on *ignitions* rather than *fires* and hence could be suppressed before beginning to
262   burn.

263   2.2.1.2 Burned area per unmanaged fire

264   After calculation of the numbers of unmanaged fires per pixel ($Fires_{UM}$), these are then
265   converted to burned area. In its original conception, INFERNO calculates the number of fires as:

266

267    $$Fires = Ignitions * Flammability \ (3)$$

268

269   In other words, both humans and lightning are conceptualised as producing ignitions,
270   which may or may not become fires based on the flammability of the surrounding vegetation. By
271   contrast, because most human fires are started deliberately, WHAM! does not output numbers of
272   *ignitions*, but numbers of *fires* directly (Figure 2). However, whilst vegetation flammability plays
273   the ontological role of translating ignitions to fires in INFERNO, it also plays an important
274   functional role: capturing geographic variation in the capacity and tendency of the vegetation to
275   sustain unmanaged fire. This is because INFERNO calculates burned area per fire with a simple
276   global mean value per Plant Functional Type. Therefore, simply removing flammability from the
277   calculation and taking numbers of unmanaged fires from WHAM! was not possible.
278

279   The solution adopted is to multiply WHAM! unmanaged fires by INFERNO
280 flammability, but to rescale with a free parameter. This leaves a burned area calculation from
281 unmanaged fires of:

282

283
$$BA_{UM} = Fires_{UM} * \Phi * \sum_{PFT=1}^{PFT=n} PFT * Flammability_{PFT} * BA_{PFT} \quad (4)$$

284 where BA_{UM} is the annual burned area from unmanaged fires as a fraction of each model pixel;
285 PFT is the fraction of each model pixel (0-1) occupied by a given PFT; $Flammability_{PFT}$ is a
286 PFT-specific dimensionless adjustment (0-1) reflecting spatiotemporal differences in the
287 combustibility of vegetation; BA_{PFT} is the PFT-specific mean burned area per fire from JULES-
288 INFERNO; and Φ is a scaling factor reflecting the differing model ontologies of WHAM! and
289 JULES-INFERNO.

290   2.2.2 Fragmentation

291   The impact of landscape fragmentation effects was restricted to unmanaged fires;
292 managed burned area was not altered for fragmentation effects, as these would already be
293 implicitly accounted for in the observations captured in DAFI. Representation of fragmentation
294 is done in three ways. Firstly, as WHAM! accounts for anthropogenic cropland fires, to account
295 for the role of cropland conversion in fragmenting more flammable fuels, burned area per
296 unmanaged fire was set to 0 for cropland PFTs.

297   Secondly, Haas et al., (2022) demonstrate the importance of road density in reducing both
298 fire sizes and burned area. This finding was implemented in the coupled model by adjusting
299 burned area per fire with a simple negative exponential function:

300

301
$$BA_{UM\_frag} = BA_{UM} * \left(1 - \frac{\ln(RD)}{\rho}\right) \quad (5)$$

302 where BA_{UM} and BA_{UM_frag} are annual burned area per pixel (0-1) from unmanaged fire before
303 and after adjustment for fragmentation effects, RD is road density and ρ a free parameter.

304   By contrast, logging of wet, fire-prone forests can lead to increased fire (both numbers of
305 fires and fire size), as gaps in the canopy lead to drying on the forest floor (Cochrane & Barber,
306 2009; Lapola et al., 2023). A simple representation of this was implemented by increasing the
307 mean burned area per fire for broadleaf tree PFTs given the presence of the Logging AFT in
308 WHAM! outputs. The values of mean burned area for broadleaf tree PFTs therefore become:

309

310
$$BA_{broadleaf}| logging = BA_{broadleaf} * \Lambda(Logging) \quad (6)$$

311 where $BA_{broadleaf}$ is the burned area per fire for broadleaf tree PFTs; $BA_{broadleaf}| logging$ is
312 this parameter value when adjusted for logging, $Logging$ is the fraction of tree cover in a cell
313 occupied by WHAM's logging AFT, and Λ a free parameter.

314   2.2.3 Combining managed and unmanaged fire

315   JULES-INFERNO typically runs at a timestep of between 30-60 minutes (Clark et al.,
316   2011). This is required for the stability of model equations and has the advantage of capturing
317   temporal fluctuations in vegetation flammability. As such, INFERNO increases the amount of
318   bare soil in a given model pixel when a fire burns, which reduces fuel availability and the
319   amount of area burned from subsequent fires until vegetation resprouts (Burton et al., 2019).
320   However, as it is not meaningful to model human land use decision-making at such short
321   durations (Arneth et al., 2014), managed fire is output at an annual timestep by WHAM!. For
322   these reasons, calculating the combined burned area of managed and unmanaged fires requires an
323   adjustment to account for the effect of preceding fires:

324

325    $$BA_{tot} = BA_{Managed} + BA_{UM} * \gamma \ (7)$$

326   where $BA_{Managed}$ is burned area from managed fire, BA_{tot} is total burned area and γ a function
327   representing the impact of preceding fires on unmanaged burned area. Managed fire was not
328   adjusted for effects of antecedent fire for several reasons: firstly, because WHAM! has its own
329   internal calculation for including fuel limitations in agent calculations; secondly, because
330   WHAM! outputs are empirically grounded, derived from data that would capture such
331   limitations to a degree. Thirdly, many managed anthropogenic fires are lit to reduce the intensity
332   and spread of unmanaged fire (e.g. prescribed fire or indigenous patch burning mosaics). The γ
333   function was calculated using a linear function after a threshold:

334

335    $$\gamma = \begin{Bmatrix} 1 \ if \ BA_{UM} \leq \alpha \\ \beta \quad otherwise \end{Bmatrix} \quad (8)$$

336   where α is a free parameter representing a threshold burned fraction of a cell below which fuel
337   availability is not limiting, whilst β is a further free parameter capturing the rate of decay in
338   burned area once this threshold is reached. This functional form was chosen as it approximates
339   the behaviour observed by Archibald et al. (2012), who explored the impact of fragmentation on
340   burned area in flammable ecosystems.

341

342   2.3 WHAM-INFERNO Calibration

343   The model structure set out in Section 2.2 resulted in 20 free parameters (Supplementary
344   Table S1), which formed the basis of a perturbed parameter ensemble for model calibration. A
345   total of 10,000 perturbed parameter sets were created with a maximin latin hypercube sampling
346   design (Carnell 2022). Using the resulting parameter sets, 10,000 model runs were conducted
347   (i.e. one for each perturbed parameter combination) for both versions of the WHAM-INFERNO
348   ensemble.
349

350   The outputs of each run were compared with the recent GFED5 global burned area
351   product (Chen et al., 2023). Firstly, 'implausible' parameter sets were ruled using history
352   matching with the overall magnitude of global burned area in GFED5. Remaining parameter sets
353   were then treated as 'not ruled out yet' (NROY; Rougier & Beven, 2013). Secondly, as well as
354   global burned area, Pearson's correlation (r) was calculated with a square root transformation
355   applied. These two metrics were those used in the FireMIP (Teckentrup et al., 2019), and hence
356   were adopted here to define a pareto-optimal parameter space capturing the trade-offs in
357   maximising performance against each metric. This approach allows, firstly, the evaluation of
358   different model processes in capturing observed fire regimes of the recent past, and secondly
359   overall evaluation of the performance of the WHAM-INFERNO ensemble. The mean outputs of
360   WI-JULES and WI-EO in the pareto parameter space then formed the basis of further analysis.
361   Fuller detail of model calibration is given in Supplementary Information A.

362

363   2.4 WHAM-INFERNO Evaluation

364   WHAM-INFERNO is evaluated in two broad ways, firstly by output corroboration
365   through comparison of model outputs with remotely sensed burned area from GFED5 (as
366   described above) and secondly by model benchmarking against a null or baseline model. The
367   baseline model was an offline version of INFERNO (as presented in Mangeon et al., 2016). As
368   INFERNO was originally calibrated using GFED4 data, in which burned area was 49% lower
369   than the more recent GFED5 burned area product, a process of recalibration required. The re-
370   calibration of this INFERNO offline model (hereafter, 'baseline model') followed broadly the
371   same steps as WHAM-INFERNO combined model: 10,000 parameter sets were used to define a
372   perturbed parameter ensemble, from which both NROY and pareto-optimal parameter spaces
373   were defined using GFED5 burned area. Detailed description of the setup of the baseline model,
374   including how its free parameters differ from WHAM-INFERNO, is described in Supplementary
375   Information A.

376

377   2.5 Historical run setup and analysis

378   As with the WHAM! standalone historical simulations presented in Perkins et al. (2023),
379   WHAM-INFERNO runs span 1990-2014. These two years mark the beginning of the data
380   recorded in the DAFI database of global anthropogenic fire impacts (i.e. 1990; Millington et al.,
381   2022) that was used to parameterise WHAM!, and the end of the CMIP6 historical period (i.e.
382   2014), respectively. Both models were run at the spatial resolution that JULES-INFERNO
383   adopted in the FireMIP (1.875° x 1.25°). Model outputs are evaluated during the overlapping
384   period in WHAM-INFERNO historical runs and the GFED5 record (2001-2014); GFED5 data
385   were aggregated to the spatial resolution of WHAM-INFERNO.

386   Analysis of outputs focuses on understanding spatial and temporal variation in the drivers
387   of global fire regimes. Spatial analysis focuses on understanding how managed anthropogenic
388   fire and unmanaged fire combine to produce observed fire regimes across global regions.
389   Similarly, temporal analysis first assessed how far managed fire and unmanaged fire contribute
390   to interannual variability in fire regimes. This was calculated by detrending the global total
391   burned area from GFED5 and WHAM-INFERNO model outputs before calculating the
392   correlation and standard deviation of the residual variabilities.

393   Then, drivers of longer-term (decadal) change were assessed. Perkins et al. (2023)
394   present analysis of the drivers of change in WHAM! managed fire outputs. Results pointed to
395   land use intensification as a global dampening effect on fire use, whilst conversely land use
396   extensification - particularly for livestock farming - led to increased fire use. Therefore, analysis
397   of temporal trends here focuses on change in unmanaged fire in relation to the human and
398   physical drivers represented in the coupled models. These are annual changes in numbers of
399   unmanaged fires, road density (fragmentation; Haas et al., 2022), vegetation flammability, fire
400   suppression and cropland conversion. The relative influence of these drivers was assessed at a
401   pixel-level firstly by comparing the Kendall's Tau correlations of their interannual changes with
402   interannual change in unmanaged burned area (for each of WI-JULES and WI-EO). Secondly,
403   using these same independent variables, linear models of pixel-level change in unmanaged
404   burned area were fit for both interannual and overall change between 2001-2014. T-values of the
405   independent variables were used to assess the relative strength of their relationships to changes in
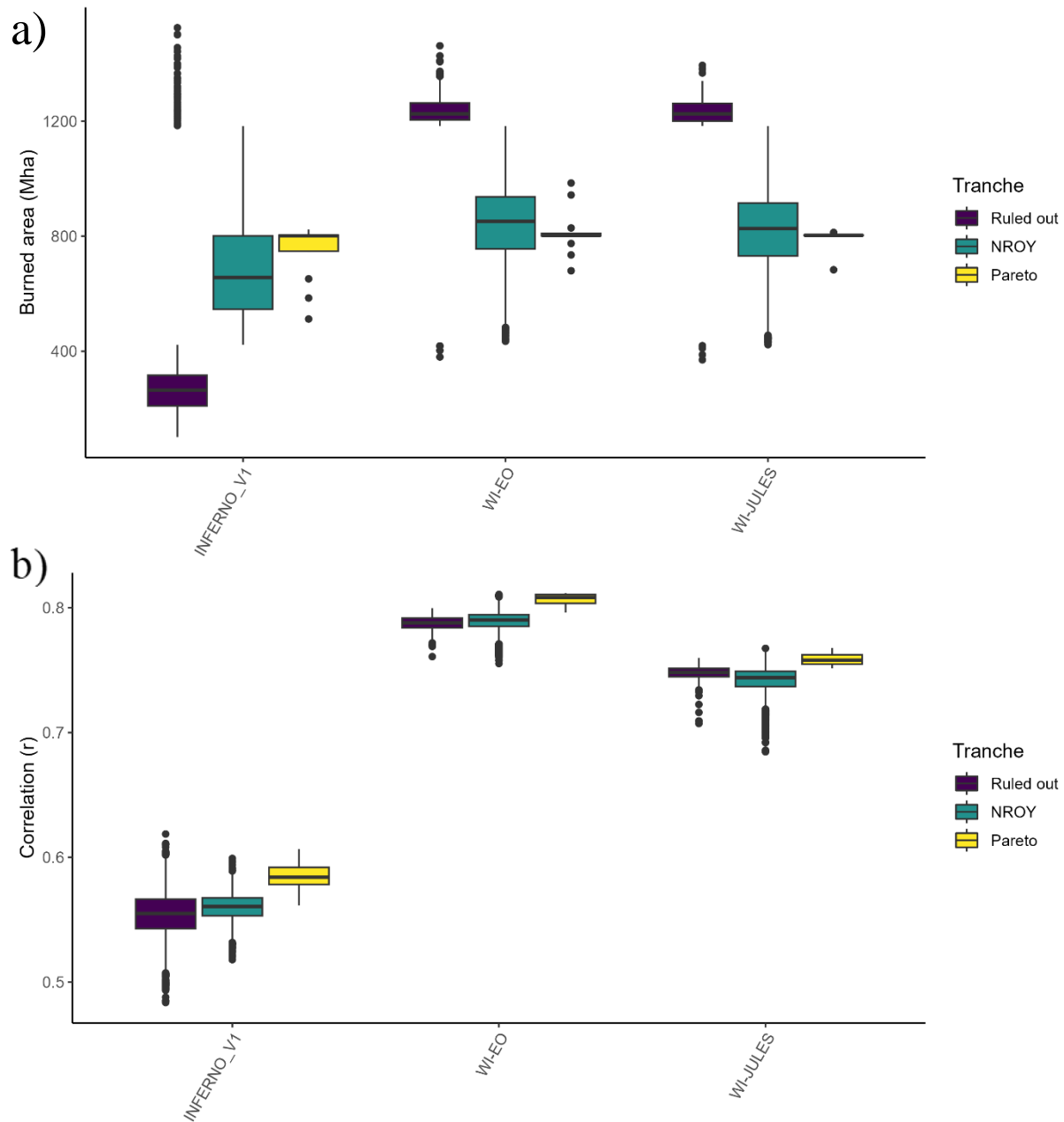406   unmanaged burned area.

407

408   **3 Results**

409   3.1 Model evaluation

410   Measured by correlation with the GFED5 record during 2001-2014, both WI-JULES and
411   WI-EO perform significantly better than the baseline model (Z Tests; both $p < 0.001$, n = 10, 14).
412   Specifically, the mean correlation of the pareto-optimal parameter space is 0.81 for WI-EO and
413   0.76 for WI-JULES, compared with 0.58 for the baseline model (Figure 3). This result also
414   compares favourably with INFERNO v1.0 presented in the FireMIP, in which INFERNO had a
415   correlation of 0.70 against GFEDv4 and 0.64 against GFEDv4s (Teckentrup et al., 2019). As
416   such, inclusion of WHAM! seemingly improves INFERNO both in an absolute sense, when
417   compared to GFED5, but also relatively against INFERNO's performance based on the
418   observational data available at the time of its original development.

419   Furthermore, almost 70% of the baseline model ensemble's runs are ruled out, primarily
420   due to simulating burned area too low to achieve acceptable coherence with the GFED5 record
421   (mean of ruled out runs was 276 Mha vs 802 Mha in GFED5). By contrast, only 182 of WI-EO
422   and 124 of WI-JULES runs are ruled out. In the pareto parameter space, WI-EO has a slight
423   overprediction bias (+11 Mha) and WI-JULES has a slight underprediction bias (-10 Mha),
424   compared to a bias of -52 Mha in the baseline model. Overall, we conclude that the WHAM
425   integration improves the structural capacity of INFERNO to capture the magnitude and
426   distribution of global fire regimes.

427

428

429 **Figure 3**: Outputs of WHAM-INFERNO in comparison with a baseline model (INFERNO_V1):
430 a) simulated global burned area and b) Pearson correlation with GFED5. For burned area, the
431 baseline model has many runs ruled out for burned area being too low in comparison with
432 GFED5, whilst in both versions of WHAM-INFERNO a smaller number of runs are ruled out.
433 The two versions of WHAM-INFERNO both produce higher correlations than the baseline
434 model across all three tranches of parameter sets (ruled out, NROY and pareto-optimal). NROY
435 refers to "not ruled out yet".
436

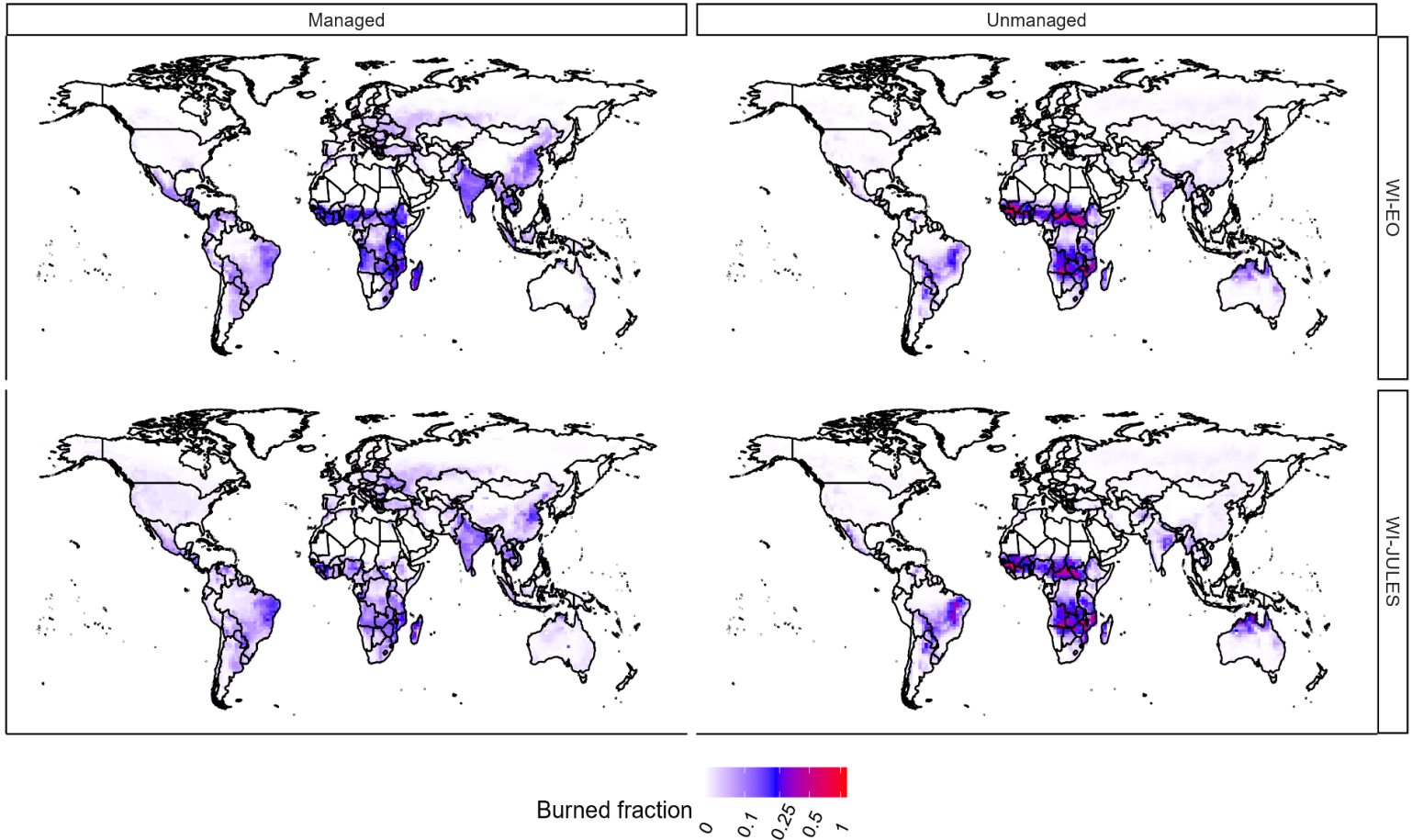437   3.2 Analysis of WHAM-INFERNO outputs

438   3.2.1 Spatial Analysis

439   Across the pareto parameter runs, simulated burned area in both coupled models is split
440 approximately evenly between managed and unmanaged fires. Over the historical period (1990-
441 2014) in WI-JULES a mean of 442 Mha (54%) comes from unmanaged fires and 379 Mha
442 (46%) from managed fires. Similarly, in WI-EO, 405 Mha (47%) comes from unmanaged fires,
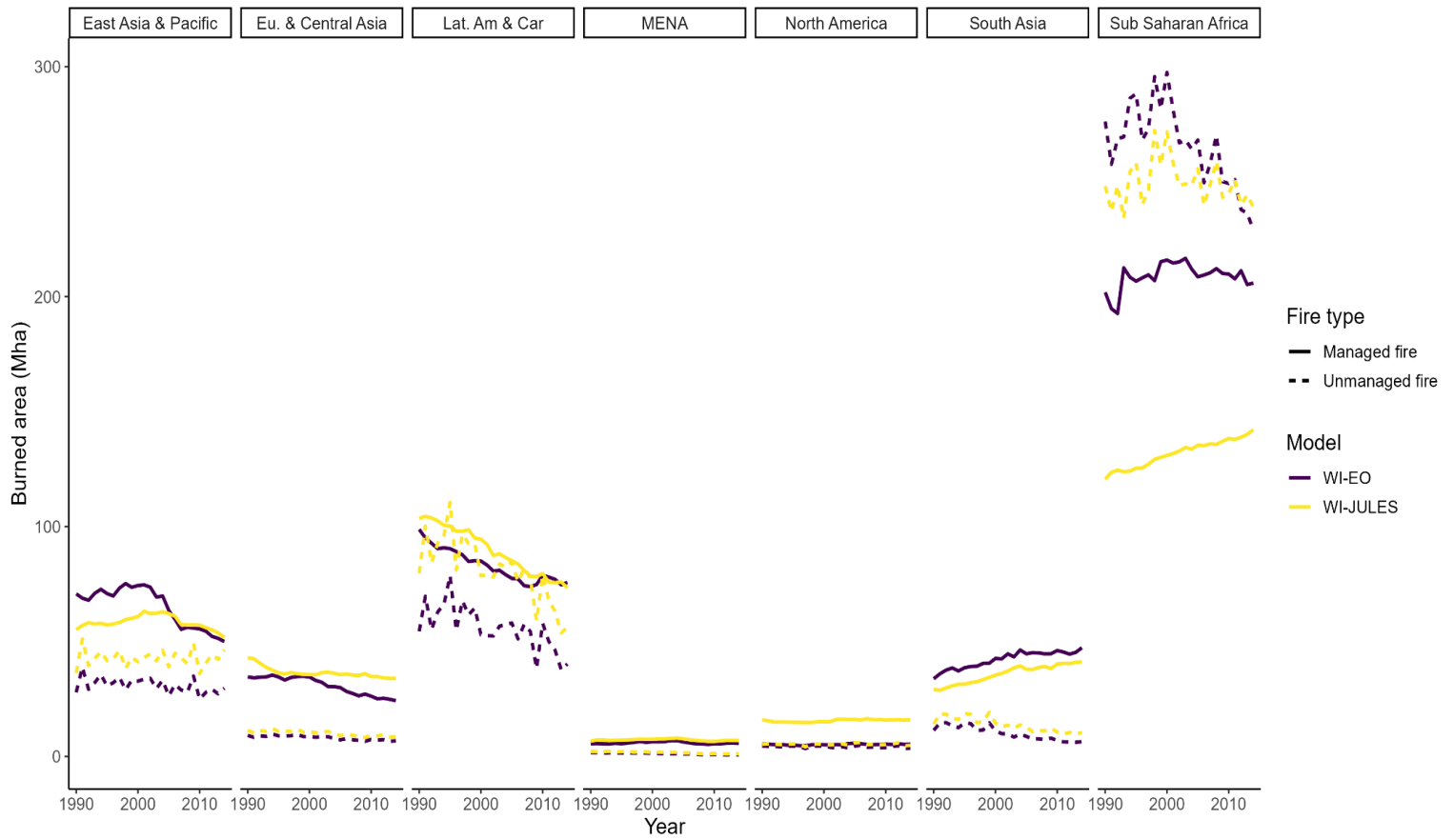443 and 453 Mha (53%) comes from managed fires.

444   Furthermore, there is substantial heterogeneity in the spatial location of burned area due
445 to managed *versus* unmanaged fires (Figure 4). For example, across 1990-2014 at the level of
446 World Bank regions, in sub-Saharan Africa WI-JULES suggests 65% of mean annual burned
447 area is from unmanaged fires (56% in WHAM-EO; Figure 5). Conversely, in South Asia (which
448 includes India), WI-JULES suggests just 28% of burned area is from unmanaged fires (19% in
449 WI-EO; Figure 5). The predominance of managed fire is driven by large-scale crop-residue
450 burning in the region (Hall et al., 2023; Perkins et al., 2023). Furthermore, there is also regional
451 heterogeneity in the trends in managed and unmanaged fire. For example, in both WI-JULES and
452 WI-EO, managed fire is increasing in South Asia, whilst decreasing in Latin America and the
453 Caribbean (Figure 5).

454   Perhaps the two most notable differences in sources of burned area between the two
455 models' (WI-JULES and WI-EO) simulations come in Latin America & the Caribbean and sub-
456 Saharan Africa. The difference in Latin America is that WI-JULES simulates higher unmanaged
457 burned area than WI-EO (81 Mha vs 56 Mha) particularly in the Caatinga region of Brazil
458 (Figure 6), which is due to a known anomaly in JULES' hydrological cycle in the region
459 (Perkins et al., 2023). By contrast, in sub-Saharan Africa WI-EO simulates higher unmanaged
460 burned area than WI-JULES (209 Mha vs 132 Mha), attributable to the more homogeneous
461 spatial distribution in WI-EO outputs – particularly in the Guinean Savanna – compared to the
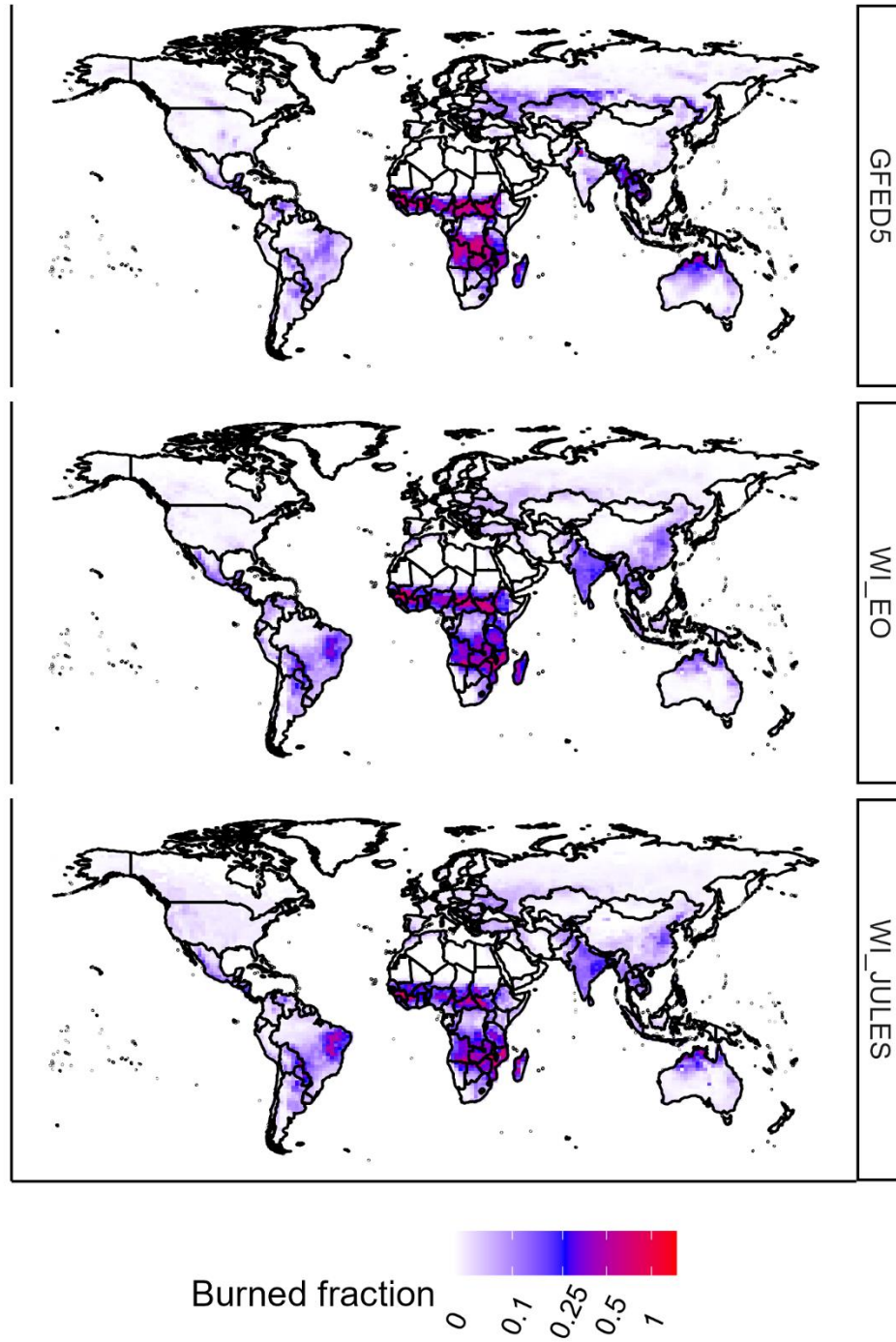462 comparatively heterogeneous WI-JULES outputs (Figures 4 & 6).
463

Figure 4: Distribution of managed and unmanaged fire in WHAM-INFERNO-Earth Observation (WI-EO) and WHAM-INFERNO-JULES (WI-JULES) shown as the burned fraction of each pixel. The arithmetic mean of model outputs was taken across the historical model run period (1990-2014). Principle differences between the two versions of WHAM-INFERNO are seen in the managed fire outputs of WI-EO in sub-Saharan Africa, which have a more homogeneous distribution than WI-JULES's more sporadic spatial pattern. Other anomalies between models are seen in the Caatinga region of Brazil and in the Northern Territories of Australia.

Figure 5: Trends in managed and unmanaged fire across the World Bank global regions. The largest gap between managed and unmanaged fire is seen in sub-Saharan Africa, where unmanaged fire dominates. Conversely, South Asia (including India) is dominated by managed fires, particularly crop residue fires (as shown in Perkins et al., 2023). Key: Eu. & Central Asia = Europe & Central Asia; Lat. Am & Car = Latin America & Caribbean; MENA = Middle East and North Africa.

Figure 6: Burned area in GFED5, WI-EO and WI-JULES as a fraction of each pixel. Values shown are the mean of the period (2001-2014). Three clear anomalies between models and GFED5 are present: firstly in the Caatinga region of Brazil, secondly in southern Russia, and thirdly in India. This latter discrepancy is due to differences in burned area from crop residue burning between WHAM! and GFED5 (Perkins et al., 2023).
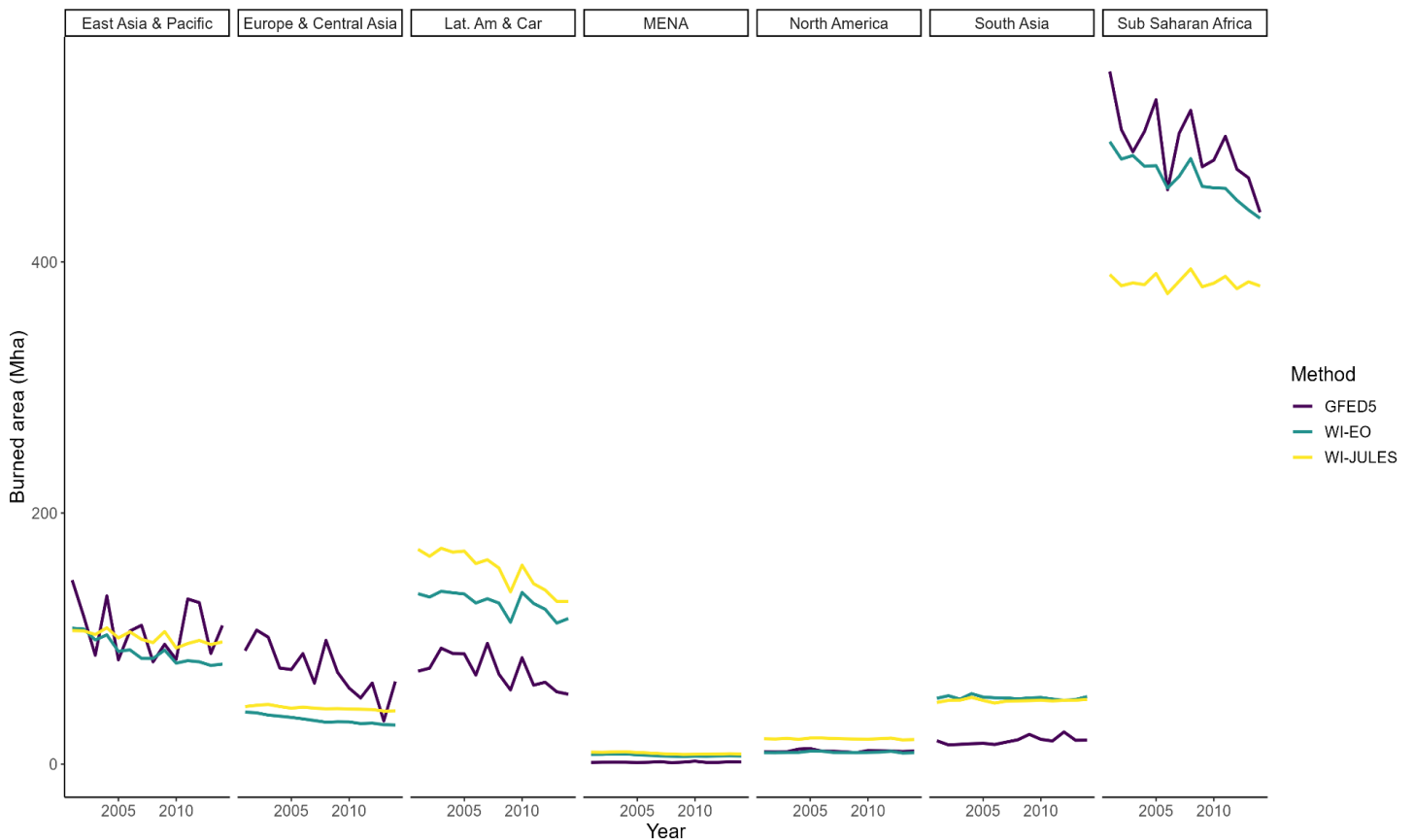
485   3.2.2 Temporal analysis

486   Across the overlapping period with GFED5 (2001-2014), WI-EO global burned area
487   declines by 137 Mha, WI-JULES burned area declines by 52 Mha, and the baseline model
488   declines by 30Mha. This compares with a decline of 193 Mha in GFED5. In WI-EO, this global
489   decline is primarily attributable to the trend in sub-Saharan Africa (Figure 7), where burned area
490   declines by 61 Mha (compared to 112 Mha in GFED5). By contrast, in WI-JULES burned area
491   in sub-Saharan Africa declines by just 9 Mha (Figure 7). This lack of decline in sub-Saharan
492   Africa is in part due to managed fires, which increase by 10 Mha as crop residue burning
493   increases in the region in this model. A similar trend is seen in sub-Saharan African crop-residue
494   burning in WI-EO, but this is offset by a steeper decline in pasture fires (Perkins et al., 2023).
495   Further, WI-JULES seemingly overestimates the rate of declining burned area in Latin America
496   & Caribbean (-42 Mha; GFED5 -18 Mha), whilst WI-EO captures a similar rate of decline to
497   GFED5 (-20 Mha). As such, WI-EO is best able to reproduce the observed decline in burned
498   area, followed by WI-JULES, and then the baseline model. The drivers of this modelled decline
499   are explored in detail below.

500   Globally, both WI-JULES and WI-EO underestimate the magnitude of interannual
501   variability (IAV) in burned area. The standard deviation of detrended model outputs (i.e. with
502   mean = 0) was 9.5Mha in WI-EO and 9.7Mha in WI-JULES. However, the correlation of the
503   detrended outputs with GFED5 was 0.81 in WI-EO and 0.41 in WI-JULES: indicating that
504   although the magnitude of IAV is underestimated in both models, WI-EO is substantially better
505   at capturing the direction of fluctuations in burned area. IAV in both model is driven by
506   unmanaged fire. Detrended global outputs for unmanaged fire correlate with detrended global
507   burned area in GFED5 (WI-EO: r = 0.74, WI-JULES: r = 0.53); however there is no meaningful
508   relationship for IAV in GFED5 and detrended outputs for managed fire (r <= 0.11).
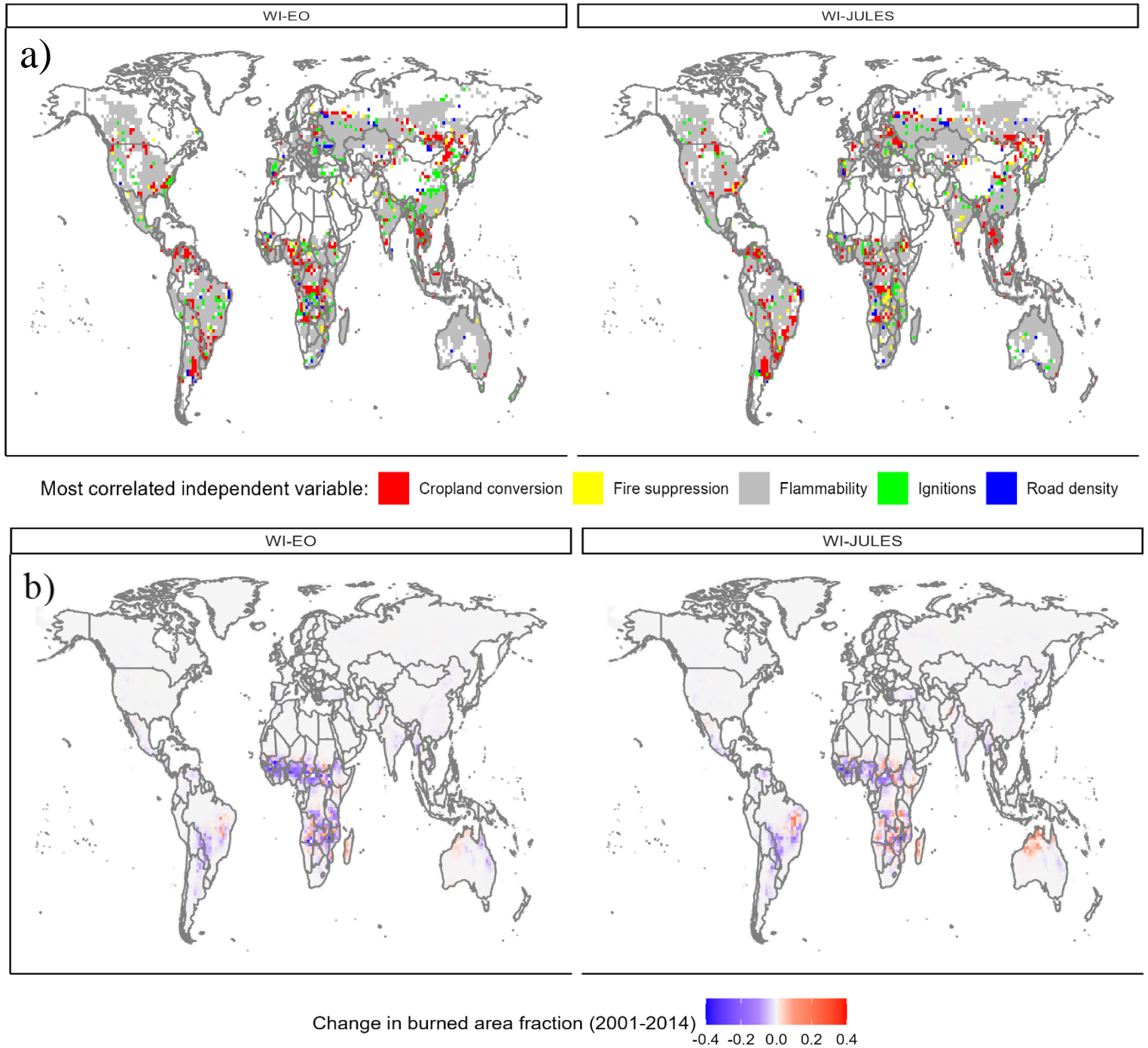
509   Based on the variable with the strongest Kendall's Tau correlation in each pixel, inter-
510   annual change in burned area due to unmanaged fire is most strongly associated with
511   flammability (Figure 8). In WI-JULES, flammability has the highest Tau value across 9,644 Mha
512   (~70% of global land area; Table 2), whilst cropland conversion, which has the strongest
513   relationship over the second largest area, has the highest Tau value across 1,037 Mha (~8% of
514   global land area). A similar trend is seen in WI-EO, where flammability has the highest Tau
515   value across 9,414 Mha and cropland conversion has the highest Tau value across 1,052 Mha.

516   However, whilst change in burned area is most closely correlated with flammability over
517   the largest area, these areas are seemingly weighted towards model pixels with less overall
518   change in burned area. For both WI-EO and WI-JULES, in linear regression models of
519   interannual variability absolute t-values for flammability are more than twice as large as any
520   other variable (Table 2). By contrast, for the overall change over 2001-2014, t-values are closer
521   between variables, with ignitions having the largest absolute t-values for both models. Similarly,
522   variables with a negative impact on burned area have a larger impact on the overall 2001-2014
523   change than interannual variation (Table 2). Road density seemingly has the largest impact on
524   declining burned area (t-values: -21.7 & -19.3), followed by cropland conversion (t-values: -16.1
525   & -19.1) respectively. Fire suppression has only a marginal influence and indeed shows little
526   relationship with the long-term trend in WI-JULES (t = 0.433).

527

528

Figure 7: Burned area by World Bank region in GFED5 and the two versions of the WHAM-INFERNO model ensemble (WHAM-EO, WI-JULES). WI-EO is best able to reproduce the observed decline in burned area in sub-Saharan Africa, with WI-JULES showing an essentially static burned area. Conversely, both WI-EO and WI-JULES overestimate burned area in Latin America, though the trend of declining burned area is captured strongly. Both models show generally poor performance in Europe & Central Asia, showing limited discernible trend. Model outputs for WI-EO and WI-JULES are the sum of the managed and unmanaged burned area presented in Figure 5. Key: Lat. Am & Car = Latin America & Caribbean; MENA = Middle East and North Africa.

Figure 8: Relationship of changes in unmanaged burned area to independent variables. a) Variable with highest absolute correlation (τ) with change in burned area from unmanaged fire; values were filtered for pixels with at least 0.1% of the land area burned. b) Change in burned area between 2001-2014. Although flammability is most closely correlated with changes in burned area across the largest geographic space, the influence of other factors – particularly cropland conversion – is clustered towards pixels with the largest changes in burned area. A non-linear stretch was applied to the colour scale in b) to show differences between smaller absolute values.

546 **Table 2**: Relationship of changes in burned area from unmanaged fires to explanatory variables.
547 Area gives the total land surface over which each variable was most strongly correlated with
548 changing burned area. T-values are from linear models of change in burned area to change in the
549 independent variable; IAV (interannual variation) is for linear models of year-on-year change
550 between 2001-2014, whilst trend denotes overall change during the same period.

551

	WI-EO (area; Mha)	WI-EO (t-value; IAV)	WI-EO (t-value; trend)	WI-JULES (area; Mha)	WI-JULES (t-value; IAV)	WI-JULES (t-value; trend)
Cropland conversion	1052	-10.4	-16.1	1037	-13.8	-19.1
Fire suppression	244	-2.78	3.26	377	-1.9	0.43
Flammability	9414	162.3	24.4	9644	267.2	46.0
Ignitions	736	70.61	25.7	522	87.5	46.6
Road density	206	-5.1	-21.7	209	-8.0	-19.3

552

4 Discussion

554 This paper has presented the first integration of a global-scale behavioural model of
555 human fire use and management coupled with a dynamic global vegetation model. Discussion
556 focuses on advances made for global understanding of human drivers of vegetation fire regimes
557 through this technical advance, before addressing its limitations and possible future directions for
558 development of WHAM-INFERNO.

559 4.1 WHAM-INFERNO: Insights for global-human fire interactions

560 The WHAM-INFERNO model integration reveals both the extent and the diversity of the
561 socio-ecological dynamics of global fire regimes. In pareto model runs of WHAM-INFERNO,
562 managed and unmanaged fire contribute approximately equal amounts of global burned area.
563 Furthermore, the spatiotemporal distribution of anthropogenic managed fire, and its relationship
564 with unmanaged ('wild') fires differs substantially across space. Whilst anthropogenic fire use,
565 primarily for crop residue burning, dominates the South Asian World Bank Region, in sub-
566 Saharan Africa more than half of burned area is from unmanaged fires (Figure 5). Such
567 differences have profound implications for understanding of global fire regimes and illustrates
568 that effective fire management policies and climate adaptation strategies must be based on
569 detailed understanding of how human livelihoods and associated fire use systems contribute to
570 existing fire regimes. At the very least, the large extent of managed anthropogenic fire around
571 the world implied by these results is demonstration of the inadequacy of model approaches
572 seeking to represent direct anthropogenic influence on fire regimes as simple functions of
573 population density (Rabin et al., 2017).
574

575   Furthermore, combined global-scale simulations of both managed and unmanaged fire
576 presented here add weight to the finding from Earth observation that small fires have declined
577 less than larger ones (Chen et al., 2023). Managed fire declines by just 35% and 52% of the rate
578 of unmanaged fire in WI-JULES and WI-EO respectively. Data from empirical studies indicates
579 that the two largest sources of burned area from managed human fires – crop residue burning and
580 pasture management – have mean sizes of 5 ha and 34 ha respectively (Millington et al., 2022),
581 whilst in JULES-INFERNO mean burned area per fire for unmanaged fires varies from 170 ha to
582 320 ha. This result seems to give weight to findings of Smith et al., (2022) and Perkins et al.,
583 (2023), that managed fire is changing in line with socio-ecological forces that are distinct from
584 those driving change in unmanaged fire.

585   In addition, the finding that unmanaged fire is primarily responsible for interannual
586 variability in burned area (Section 3.2.2) is consistent with the findings of Randerson et al.,
587 (2012), who find less fluctuation in small fires than those detectable by MODIS (i.e. <21 ha).
588 This is intuitive, as crop residue fires, for example, occur annually according to the logic of
589 cropping systems rather than fluctuations in climate (Millington et al., 2022). However, this
590 opens an intriguing possibility for fire-enabled DGVMs, which have typically struggled with
591 interannual variability whilst also not including representation of managed human fires – the
592 more static part of the regime (Li et al., 2019). In effect, DGVMs may have been *doubly*
593 underestimating the sensitivity of burned area from unmanaged fires to interannual climate
594 variability. This underrepresentation of the sensitivity of unmanaged fires to climate volatility
595 may contribute to the difficulty of attributing changes in global fire regimes to global warming
596 (Jones et al., 2022), although a lack of representation of peat fires may also be a partial
597 explanation (Blackford et al., 2023; Li et al., 2019).

598   By accounting for the less temporally variable and more spatially homogeneous signal of
599 burned area due to managed fires (Figures 4 & 5), the WHAM-INFERNO integration advances
600 understanding of the drivers of declining global burned area. Whilst interannual variability is
601 primarily driven by changes in vegetation flammability, longer-term change in burned area
602 highlights the important role played by the fragmentation of natural and semi-natural vegetation
603 through road building and cropland conversion (Figure 8). This result coheres strongly with that
604 of Andela et al., (2017) who find that interannual variability is closely linked to precipitation,
605 whilst cropland fraction is strongly associated with declining burned area. Furthermore, WHAM-
606 INFERNO can identify the processes underlying the finding of Andela that cropland has a
607 spatially heterogeneous impact on burned area. For example, increased burned area in croplands
608 in South Asia and Northeastern China is due to large-scale agricultural residue burning, whilst
609 decreased fire in savanna grasslands is due to landscape fragmentation and the subsequent
610 reduced capacity of savanna grasslands to sustain unmanaged fires.

611

4.2 Model performance and limitations

Both versions of the WHAM-INFERNO ensemble represent a significant improvement in the capacity of INFERNO to reproduce historical global annual burned area over the baseline model (Figure 3), and indeed over the performance of INFERNO against GFED4 presented in FIREMIP (r= 0.70; Mangeon et al., 2016; Teckentrup et al., 2019). This demonstrates the fundamental importance of a process-based approach to understanding and representing human-fire interactions in global modelling. Furthermore, the improvements made in WHAM-INFERNO over the baseline version allow the impact of landscape fragmentation in global burned area to be incorporated and understood (Figures 2 & 8). Indeed, the WHAM-INFERNO integration, and particular WI-EO seems to advance capacity for DGVMs to reproduce the observed decline in global burned area (Hantson et al., 2020).

However, representation of landscape fragmentation, its interaction with different ecosystem types, and other anthropogenic pressures remains incomplete. One way that WHAM-INFERNO represents fragmentation is through the role of roads in reducing fire size (Haas et al., 2022), by applying a road density correction to fire sizes per PFT. Although useful in constraining the model pareto parameter space through restricting burned area in more densely populated areas (Supplementary Information; Figure S1) this single global function is a somewhat simplistic way of capturing such effects, resulting in a substantially larger impact on WHAM-INFERNO burned area outputs than on correlation with GFED5 (Supplementary Information; Figure S2). Hence, the road density parameterisation in WHAM-INFERNO employed to capture fragmentation effects is analogous to representations of anthropogenic 'ignitions' as a global function of population density in previous fire-enabled DGVMs: they are both a first step with outstanding issues to be addressed. By contrast, the representation of selective logging on the flammability of fire-prone tropical forests in WHAM-INFERNO has been more successful. Although having a small impact on global burned area, including this process leads to an improved global correlation between WHAM-INFERNO outputs and GFED5 (Supplementary Information; Figure S2). Representation of logging was derived from WHAM! outputs, hence illustrating the value of process-based representation of anthropogenic impacts on fire regimes, as opposed to the top-down road density parameterisation.

Finally, it is notable that WI-EO performs more strongly than WI-JULES at reproducing the magnitude, spatial distribution and temporal dynamics of burned area found in GFED5. On one hand, this illustrates the benefits of a well-specified parameterisation of managed human fire: by better accounting for this aspect of the observed burned area signal, WI-EO is better able to reproduce the inter-annual variability of unmanaged fire, and its pronounced global decline. Yet the weaker performance of WI-JULES perhaps also illustrates the potential for underlying error in the representation of ecosystems within DGVMs to lead to misleading conclusions being drawn from their fire modules (Hantson et a., 2020). Continued model intercomparison projects and use of model ensembles are likely to remain the most effective means to apply the fire outputs of DGVMs (e.g. Burton et al., 2023). Overall, the large scale of anthropogenic managed fire entails that careful consideration should be given to how future socioeconomic scenarios, and their limitations, inform our projections of how global fire regimes may evolve under a warming climate (Keys et al., 2024).

5 Conclusion

This paper has presented the first integration of a global behavioural model of human fire use and management with a dynamic global vegetation model. Overall, model evaluation highlights the strong benefits of coupled socio-ecological modelling approaches for reproducing the observed spatial and temporal patterns of burned area globally. Furthermore, findings demonstrate the extent and complexity of human-fire interactions. Results imply that managed anthropogenic fire accounts for as much as half of all global burned area, whilst the trends and distribution of, and relationship between, managed and unmanaged fires is highly spatially heterogeneous. Such complexities demonstrate that socio-ecological modelling is vital to advance understanding of present-day and future fire regimes. A key area for future work identified here is in developing more nuanced representation of landscape fragmentation, particularly in grazing lands in sub-Saharan Africa, which remain a central contributor to global burned area.

Open Research

Data and code necessary to reproduce the results in this paper, as well as analysis and figures presented are made available on zenodo: https://zenodo.org/doi/10.5281/zenodo.8319445 (Perkins et al., 2023b). Code to run the WHAM-INFERNO ensemble are also made available on GitHub: https://github.com/OliPerkins1987/WHAM_INFERNO. All data and code are mode available under a Creative Commons License.

References

Andela, N., Morton, D. C., Giglio, L., Chen, Y., van der Werf, G. R., Kasibhatla, P. S., et al. (2017). A human-driven decline in global burned area. *Science*, *356*(6345), 1356–1362. https://doi.org/10.1126/science.aal4108

Archibald, S. (2016). Managing the human component of fire regimes: Lessons from Africa. *Philosophical Transactions of the Royal Society B: Biological Sciences*, *371*(1696), 20150346. https://doi.org/10.1098/rstb.2015.0346

Archibald, S., & Hempson, G. P. (2016). Competing consumers: Contrasting the patterns and impacts of fire and mammalian herbivory in Africa. *Philosophical Transactions of the Royal Society B: Biological Sciences*, *371*(1703), 20150309. https://doi.org/10.1098/rstb.2015.0309

Archibald, S., Staver, A. C., & Levin, S. A. (2012). Evolution of human-driven fire regimes in Africa. *Proceedings of the National Academy of Sciences*, *109*(3), 847–852. https://doi.org/10.1073/pnas.1118648109

Arneth, A., Brown, C., & Rounsevell, M. D. A. (2014). Global models of human decision-making for land-based mitigation and adaptation assessment. *Nature Climate Change*, *4*(7), Article 7. https://doi.org/10.1038/nclimate2250

Blackford, K. R., Kasoar, M., Burton, C., Burke, E., Prentice, I. C., & Voulgarakis, A. (2023). INFERNO-peat v1.0.0: A representation of northern high latitude peat fires in the JULES-INFERNO global fire model. *EGUsphere*, 1–31. https://doi.org/10.5194/egusphere-2023-2399

Burton, C., Betts, R., Cardoso, M., Feldpausch, T. R., Harper, A., Jones, C. D., et al. (2019). Representation of fire, land-use change and vegetation dynamics in the Joint UK Land Environment Simulator vn4.9 (JULES). *Geoscientific Model Development*, *12*(1), 179–193. https://doi.org/10.5194/gmd-12-179-2019

Burton, C., Lampe, S., Kelley, D., Thiery, W., Hantson, S., Christidis, N., et al. (2023). Global burned area increasingly explained by climate change, PREPRINT (Version 1) available at Research Square. https://doi.org/10.21203/rs.3.rs-3168150/v1

Carnell, R. (2022). *lhs: Latin Hypercube Samples*. R package version 1.1.6, https://CRAN.R-project.org/package=lhs.

Chen, Y., Hall, J., van Wees, D., Andela, N., Hantson, S., Giglio, L., et al. (2023). Multi-decadal trends and variability in burned area from the 5th version of the Global Fire Emissions Database (GFED5). *Earth System Science Data Discussions*, 1–52. https://doi.org/10.5194/essd-2023-182

Christian, H. J., Blakeslee, R. J., Boccippio, D. J., Boeck, W. L., Buechler, D. E., Driscoll, K. T., et al. (2003). Global frequency and distribution of lightning as observed from space by the Optical Transient Detector. *Journal of Geophysical Research: Atmospheres*, *108*(D1), ACL 4-1-ACL 4-15. https://doi.org/10.1029/2002JD002347

Clark, D. B., Mercado, L. M., Sitch, S., Jones, C. D., Gedney, N., Best, M. J., et al. (2011). The Joint UK Land Environment Simulator (JULES), model description – Part 2: Carbon fluxes and vegetation dynamics. *Geoscientific Model Development*, *4*(3), 701–722. https://doi.org/10.5194/gmd-4-701-2011

Cochrane, M. A., & Barber, C. P. (2009). Climate change, human land use and future fires in the Amazon. *Global Change Biology*, *15*(3), 601–612. https://doi.org/10.1111/j.1365-2486.2008.01786.x

Driscoll, D. A., Armenteras, D., Bennett, A. F., Brotons, L., Clarke, M. F., Doherty, T. S., et al. (2021). How fire interacts with habitat loss and fragmentation. *Biological Reviews*, *96*(3), 976–998. https://doi.org/10.1111/brv.12687

Ford, A. E., Harrison, S. P., Kountouris, Y., Millington, J. D., Mistry, J., Perkins, O., et al. (2021). Modelling human-fire interactions: Combining alternative perspectives and approaches. *Frontiers in Environmental Science*, *9*, 649835.

Forkel, M., Andela, N., Harrison, S. P., Lasslop, G., van Marle, M., Chuvieco, E., et al. (2019). Emergent relationships with respect to burned area in global satellite observations and fire-enabled vegetation models. *Biogeosciences*, *16*(1), 57–76. https://doi.org/10.5194/bg-16-57-2019

736 Giglio, L., Randerson, J. T., & van der Werf, G. R. (2013). Analysis of daily, monthly, and
737   annual burned area using the fourth-generation global fire emissions database (GFED4).
738   *Journal of Geophysical Research: Biogeosciences*, *118*(1), 317–328.
739   https://doi.org/10.1002/jgrg.20042

740 Haas, O., Prentice, I. C., & Harrison, S. P. (2022). Global environmental controls on wildfire
741   burnt area, size, and intensity. *Environmental Research Letters*, *17*(6), 065004.
742   https://doi.org/10.1088/1748-9326/ac6a69

743 Hall, J., Argueta, F., Zubkova, M., Chen, Y., Randerson, J. & Giglio, L. (2024). GloCAB: global
744   cropland burned area from mid-2002 to 2020. *Earth System Science Data*, 16(2), 867-
745   885. https://doi.org/10.5194/essd-16-867-2024

746 Hantson, S., Kelley, D. I., Arneth, A., Harrison, S. P., Archibald, S., Bachelet, D., et al. (2020).
747   Quantitative assessment of fire and vegetation properties in simulations with fire-enabled
748   vegetation models from the Fire Model Intercomparison Project. *Geoscientific Model*
749   *Development*, *13*(7), 3299–3318.

750 Harrison, S. P., Prentice, I. C., Bloomfield, K. J., Dong, N., Forkel, M., Forrest, M., et al. (2021).
751   Understanding and modelling wildfire regimes: An ecological perspective.
752   *Environmental Research Letters*, *16*(12), 125008. https://doi.org/10.1088/1748-
753   9326/ac39be

754 Hijmans, R. (2023). raster: Geographic Data Analysis and Modeling. R package version 3.6-20.
755   https://CRAN.R-project.org/package=raster

756 Hurtt, G. C., Chini, L., Sahajpal, R., Frolking, S., Bodirsky, B. L., Calvin, K., et al. (2020).
757   Harmonization of global land use change and management for the period 850–2100
758   (LUH2) for CMIP6. *Geoscientific Model Development*, *13*(11), 5425–5464.
759   https://doi.org/10.5194/gmd-13-5425-2020

760 Jones, M. W., Abatzoglou, J. T., Veraverbeke, S., Andela, N., Lasslop, G., Forkel, M., et al.
761   (2022). Global and Regional Trends and Drivers of Fire Under Climate Change. *Reviews*
762   *of Geophysics*, *60*(3), e2020RG000726. https://doi.org/10.1029/2020RG000726

763 Kelley, D. I., Bistinas, I., Whitley, R., Burton, C., Marthews, T. R., & Dong, N. (2019). How
764   contemporary bioclimatic and human controls change global fire regimes. *Nature*
765   *Climate Change*, *9*(9), 690–696. https://doi.org/10.1038/s41558-019-0540-7

766 Keys, P. W., Badia, L., & Warrier, R. (2024). The Future in Anthropocene Science. *Earth's*
767   *Future*, *12*(1), e2023EF003820. https://doi.org/10.1029/2023EF003820

768 Kumar, N., Chaudhary, A., Ahlawat, O. P., Naorem, A., Upadhyay, G., Chhokar, R. S., et al.
769   (2023). Crop residue management challenges, opportunities and way forward for
770   sustainable food-energy security in India: A review. *Soil and Tillage Research*, *228*,
771   105641. https://doi.org/10.1016/j.still.2023.105641

772 Lapola, D. M., Pinho, P., Barlow, J., Aragão, L. E. O. C., Berenguer, E., Carmenta, R., et al.
773   (2023). The drivers and impacts of Amazon forest degradation. *Science*, *379*(6630),
774   eabp8622. https://doi.org/10.1126/science.abp8622

775   Laris, P. (2002). Burning the Seasonal Mosaic: Preventative Burning Strategies in the Wooded
776   Savanna of Southern Mali. *Human Ecology*, *30*(2), 155–186.
777   https://doi.org/10.1023/A:1015685529180

778   Lasslop, G., Coppola, A., Voulgarakis, A., Yue, C., & Veraverbeke, S. (2019). Influence of Fire
779   on the Carbon Cycle and Climate. *Current Climate Change Reports*, 5, 112-113.
780   https://doi.org/10.1007/s40641-019-00128-9

781   Li, F., Val Martin, M., Andreae, M. O., Arneth, A., Hantson, S., Kaiser, J. W., et al. (2019).
782   Historical (1700–2012) global multi-model estimates of the fire emissions from the Fire
783   Modeling Intercomparison Project (FireMIP). *Atmospheric Chemistry and Physics*,
784   *19*(19), 12545–12567. https://doi.org/10.5194/acp-19-12545-2019

785   Mangeon, S., Voulgarakis, A., Gilham, R., Harper, A., Sitch, S., & Folberth, G. (2016).
786   INFERNO: A fire and emissions scheme for the UK Met Office's Unified Model.
787   *Geoscientific Model Development*, *9*(8), 2685–2700. https://doi.org/10.5194/gmd-9-2685-
788   2016

789   Mathison, C., Burke, E., Hartley, A. J., Kelley, D. I., Burton, C., Robertson, E., et al. (2023).
790   Description and evaluation of the JULES-ES set-up for ISIMIP2b. *Geoscientific Model
791   Development*, *16*(14), 4249–4264. https://doi.org/10.5194/gmd-16-4249-2023

792   Meijer, J. R., Huijbregts, M. A. J., Schotten, K. C. G. J., & Schipper, A. M. (2018). Global
793   patterns of current and future road infrastructure. *Environmental Research Letters*, *13*(6),
794   064006. https://doi.org/10.1088/1748-9326/aabd42

795   Millington, J. D. A., Perkins, O., & Smith, C. (2022). Human Fire Use and Management: A
796   Global Database of Anthropogenic Fire Impacts for Modelling. *Fire*, *5*(4), Article 4.
797   https://doi.org/10.3390/fire5040087

798   Perkins, O., Kasoar, M., Voulgarakis, A., Smith, C., Mistry, J., & Millington, J. (2023). A global
799   behavioural model of human fire use and management: WHAM! v1.0. *EGUsphere*
800   (accepted for publication in *Geoscientific Model Development*), 1–42.
801   https://doi.org/10.5194/egusphere-2023-2162.

802   Perkins, O., Kasoar, M., Voulgarakis, A., Edwards, T., & Millington, J. (2023b). [Software]
803   WHAM-INFERNO, code and supporting data.
804   https://zenodo.org/doi/10.5281/zenodo.8319445

805   Perkins, O., & Millington, J. D. A. (2021). DAFI: A global database of Anthropogenic Fire.
806   *Figshare Https://Doi. Org/10.6084/M9. Figshare. c*, *5290792*.

807   R Core Team. (2022). R: A language and environment for statistical computing. R Foundation
808   for Statistical Computing, Vienna, Austria. https://www.R-project.org/.

809   Rabin, S. S., Melton, J. R., Lasslop, G., Bachelet, D., Forrest, M., Hantson, S., et al. (2017). The
810   Fire Modeling Intercomparison Project (FireMIP), phase 1: Experimental and analytical
811   protocols with detailed model descriptions. *Geoscientific Model Development*, *10*(3),
812   1175–1197. https://doi.org/10.5194/gmd-10-1175-2017

813   Randerson, J. T., Chen, Y., van der Werf, G. R., Rogers, B. M., & Morton, D. C. (2012). Global
814   burned area and biomass burning emissions from small fires. *Journal of Geophysical
815   Research: Biogeosciences*, *117*(G4). https://doi.org/10.1029/2012JG002128

816 Ripley, B. S., Raubenheimer, S. L., Perumal, L., Anderson, M., Mostert, E., Kgope, B. S.,
817   Midgley, G. F., & Simpson, K. J. (2022). CO2-fertilisation enhances resilience to
818   browsing in the recruitment phase of an encroaching savanna tree. *Functional Ecology*,
819   *36*(12), 3223–3233. https://doi.org/10.1111/1365-2435.14215

820 Robinson, D. T., Di Vittorio, A., Alexander, P., Arneth, A., Barton, C. M., Brown, D. G.,
821   Kettner, A., Lemmen, C., et al. (2018). Modelling feedbacks between human and natural
822   processes in the land system. *Earth System Dynamics*, *9*(2), 895–914.
823   https://doi.org/10.5194/esd-9-895-2018

824 Rosan, T. M., Sitch, S., Mercado, L. M., Heinrich, V., Friedlingstein, P., & Aragão, L. E. O. C.
825   (2022). Fragmentation-Driven Divergent Trends in Burned Area in Amazonia and
826   Cerrado. *Frontiers in Forests and Global Change*, *5*.
827   https://www.frontiersin.org/articles/10.3389/ffgc.2022.801408

828 Rougier, J. C., & Beven, K. J. (2013). *Model and data limitations: The sources and implications
829   of epistemic uncertainty* (pp. 40–63). Cambridge University Press.
830   https://doi.org/10.1017/CBO9781139047562.004

831 Shuman, J. K., Balch, J. K., Barnes, R. T., Higuera, P. E., Roos, C. I., Schwilk, D. W., et al.
832   (2022). Reimagine fire science for the anthropocene. *PNAS Nexus*, *1*(3), pgac115.
833   https://doi.org/10.1093/pnasnexus/pgac115

834 Smith, C., Perkins, O., & Mistry, J. (2022). Global decline in subsistence-oriented and
835   smallholder fire use. *Nature Sustainability*, *5*(6), Article 6.
836   https://doi.org/10.1038/s41893-022-00867-y

837 Stevens, N., Erasmus, B. F. N., Archibald, S., & Bond, W. J. (2016). Woody encroachment over
838   70 years in South African savannahs: Overgrazing, global change or extinction
839   aftershock? *Philosophical Transactions of the Royal Society B: Biological Sciences*,
840   *371*(1703), 20150437. https://doi.org/10.1098/rstb.2015.0437

841 Teckentrup, L., Harrison, S. P., Hantson, S., Heil, A., Melton, J. R., Forrest, M., et al. (2019).
842   Response of simulated burned area to historical changes in environmental and
843   anthropogenic factors: A comparison of seven fire models. *Biogeosciences*, *16*(19),
844   3883–3910. https://doi.org/10.5194/bg-16-3883-2019

845 UNEP - the United Nations Environment Programme (2022). *Spreading like Wildfire: The
846   Rising Threat of Extraordinary Landscape Fires*.
847   http://www.unep.org/resources/report/spreading-wildfire-rising-threat-extraordinary-
848   landscape-fires

849 Wiltshire, A. J., Duran Rojas, M. C., Edwards, J. M., Gedney, N., Harper, A. B., Hartley, A. J.,
850   et al. (2020). JULES-GL7: The Global Land configuration of the Joint UK Land
851   Environment Simulator version 7.0 and 7.2. *Geoscientific Model Development*, *13*(2),
852   483–505. https://doi.org/10.5194/gmd-13-483-2020

853 Zubkova, M., Humber, M. L., & Giglio, L. (2023). Is global burned area declining due to
854   cropland expansion? How much do we know based on remotely sensed data?
855   *International Journal of Remote Sensing*, *44*(4), 1132–1150.
856   https://doi.org/10.1080/01431161.2023.2174389

857

References from the supporting information

Craig, P.S., Goldstein, M., Seheult, A.H., & Smith, J.A. (1997). P*ressure Matching for Hydrocarbon Reservoirs: A Case Study in the Use of Bayes Linear Strategies for Large Computer Experiments*, in: Gatsonis, C., Hodges, J.S., Kass, R.E., McCulloch, R., Rossi, P., Singpurwalla, N.D. (Eds.), *Case Studies in Bayesian Statistics*, Lecture Notes in Statistics. Springer, New York, NY, pp. 37–93. https://doi.org/10.1007/978-1-4612-2290-3_2

Florian, A. (1992). An efficient sampling scheme: Updated Latin Hypercube Sampling. *Probabilistic Engineering Mechanics*, 7, 123–130. https://doi.org/10.1016/0266-8920(92)90015-A

Gupta, H.V., Sorooshian, S., & Yapo, P.O., 1998. Toward improved calibration of hydrologic models: Multiple and noncommensurable measures of information. *Water Resources Research*, 34, 751–763. https://doi.org/10.1029/97WR03495

Kennedy, M., & O'Hagan, A. (2001). Bayesian calibration of computer models, *Journal of the Royal Statistical Society* B, 63:3, 425-464.

Lin, Y., Xu, D., Wang, N., Shi, Z., & Chen, Q. (2020). Road Extraction from Very-High-Resolution Remote Sensing Images via a Nested SE-Deeplab Model. *Remote Sensing*, 12, 2985. https://doi.org/10.3390/rs12182985

Lu, L., Anderson-Cook, C.M., & Robinson, T.J. (2011). Optimization of Designed Experiments Based on Multiple Criteria Utilizing a Pareto Frontier. *Technometrics*, 53, 353–365.

McNeall, D., Williams, J., Booth, B., Betts, R., Challenor, P., Wiltshire, A., & Sexton, D. (2016). The impact of structural error on parameter constraint in a climate model. *Earth System Dynamics*, 7, 917–935. https://doi.org/10.5194/esd-7-917-2016

Pukelsheim, F. (1994). The Three Sigma Rule. *The American Statistician*, 48, 88–91. https://doi.org/10.2307/2684253

Roteta, E., Bastarrika, A., Padilla, M., Storm, T., & Chuvieco, E. (2019). Development of a Sentinel-2 burned area algorithm: Generation of a small fire database for sub-Saharan Africa. *Remote Sensing of Environment*, 222, 1–17. https://doi.org/10.1016/j.rse.2018.12.011

Williamson, D., Goldstein, M., Allison, L., Blaker, A., Challenor, P., Jackson, L., & Yamazaki, K. (2013). History matching for exploring and reducing climate model parameter space using observations and a large perturbed physics ensemble. *Climate Dynamics*, 41, 1703–1729. https://doi.org/10.1007/s00382-013-1896-4